

Chemical and spectroscopic characterization of humic acids extracted from the bottom sediments of a Brazilian subtropical microbasin

**M. Giovanela^{a*}, J. S. Crespo^a, M. Antunes^a, D. S. Adamatti^a, A. N. Fernandes^a,
A. Barison^b, C. W. P. da Silva^b, R. Guégan^c, M. Motelica-Heino^c, M. M. D. Sierra^d**

^aCentro de Ciências Exatas e Tecnologia, Universidade de Caxias do Sul, 95070-560 Caxias do Sul, RS, Brazil.

^bDepartamento de Química, Universidade Federal do Paraná, 81531-990 Curitiba, PR, Brazil.

^cInstitut des Sciences de la Terre, CNRS UMR 6113, Université d'Orléans, 45071 Orléans Cedex 2, France.

^dDepartamento de Química, Universidade Federal de Santa Catarina, 88040-900 Florianópolis, SC, Brazil.

*E-mail address: mgiovan1@ucs.br (M. Giovanela).

Abstract

Humic substances (HS) perform a fundamental role in aquatic environments, exhibiting different levels of reactivity in retaining metal ions and organic pollutants. Also, they control the primary production of these ecosystems and act in the carbon sequestering process. In order to improve our understanding vis-à-vis the structural and functional features of HS from aquatic systems, this study aimed to chemically and spectroscopically characterize humic acids (HA) isolated from bottom sediment samples of a stream in a Brazilian subtropical microbasin by elemental analysis, and infrared (FT-IR), ultraviolet and visible (UV-Vis) and solid-state ^{13}C nuclear magnetic resonance (CP-MAS ^{13}C NMR) spectroscopies, thermogravimetry (TG), and scanning electron microscopy (SEM). Although all samples originated from the same environment, the data showed that the HA have distinct chemical and spectroscopic properties, and that the location and characteristics of the sampling points from which the sediments were collected played an important role in the differences observed. Furthermore, vascular plant matter is probably the main contributor to these samples.

Key-words: subtropical microbasin; sediments; humic acids; elemental and spectroscopic analyses.

1. Introduction

Humic substances (HS) are ubiquitous natural materials occurring in soils, sediments and water as a product of the chemical and biological transformation of animal and plant residues [1]. They represent a significant proportion of the organic carbon cycle on earth having, consequently, a profound influence on the biogeochemical cycles of both natural and anthropogenic constituents [2]. Based on their solubility in aqueous solution, HS are operationally divided into three different fractions: (i) humic acid (HA), the fraction soluble at alkaline pH values; (ii) fulvic acid (FA), the fraction soluble at all pH values; and (iii) humin, the fraction insoluble at all pH values [3].

The newest concept attributed to HS is that they consist of associations of relatively small molecules with similar characteristics, held together via supramolecular interactions [4]. Due to their substantial impact on a variety of environmental processes, knowledge of the physical and chemical properties of these substances, as well as of their interactions with xenobiotics, are aspects that should always be considered in studies related to the management and remediation of impacted ecosystems.

A detailed characterization of HS and their manifold processes in the environment requires the application of several analytical tools combined with chemical and spectroscopic methods. Elemental analysis is the first step in any such study. The H/C and C/N atomic ratios can then be used to indicate the organic matter (OM) source, the degree of condensation, and the environmental conditions under which the HS were generated [5–7].

Fourier Transform Infrared (FT-IR) spectroscopy has also been extensively used

in investigations related to HA and has provided considerable insight into the nature, reactivity and structural arrangement of oxygen-containing functional groups in HS [8–10]. The resulting IR spectra contain a variety of bands that are indicative of the different functional groups present in these complex mixtures.

UV-Visible (UV-Vis) spectroscopy is another technique which can provide useful information on the composition and origin of OM [11–13]. Within this context, some numerical indexes derived employing this technique has been proposed in the literature. Classical parameters such as the ratio between the absorbance at 465 nm and 665 nm (E_4/E_6) and the $\Delta \log K$ coefficient ($\log \text{Abs}_{400 \text{ nm}} - \log \text{Abs}_{600 \text{ nm}}$) have proven to be useful to evaluate the degree of humification of HS extracted from organic materials of diverse origins [14–16].

Nuclear magnetic resonance spectroscopy of carbon isotope 13 (^{13}C NMR), especially in solid state, under cross-polarization and magic angle spinning (CP-MAS) conditions, has been employed to investigate the functionality of HA both qualitatively and quantitatively and to distinguish between different functional groups [10, 17–19].

Thermal analysis represents a rapid, accurate and interference-free approach, which is thus applicable in the investigation of complex materials such as HA and related humified substrates. In HS studies, thermogravimetry (TG) and derivative thermogravimetry (DTG) have both been applied to quantify the moisture and ash contents [20], as well as to observe and characterize structural changes in the samples during heating [21].

Finally, scanning electron microscopy (SEM) has been widely used to observe the microstructure of organic soil components, including HS, and their associations with inorganic material [22–24].

With the aim of improving our understanding vis-à-vis the structural and functional features of HS from aquatic systems, the goal of this paper is to discuss the detailed chemical properties of HA isolated from four bottom sediment samples collected from a stream in a Brazilian subtropical microbasin. Analysis was carried out applying a combination of chemical and spectroscopic techniques including SEM, CHNO-S analysis, TG, and UV-Vis, FT-IR, and CP-MAS ^{13}C NMR spectroscopies.

2. Materials and methods

2.1 Chemicals

The chemicals were of analytical-grade quality and purchased directly from Merck. All aqueous solutions were prepared with deionized water (18.2 M Ω /cm resistivity) obtained from a Milli-Q system (Millipore).

2.2 Cleaning glassware and plasticware

All laboratory glassware and plasticware used in the sampling and preservation of sediment samples, as well as in the extraction of the HA, was firstly washed with tap water and then soaked in an alkaline Extran solution (15% v/v) for 24 h. After this period, they were washed thoroughly with tap water and then soaked in a solution of HNO₃ (50% v/v) for 48 h. Finally, the material was rinsed with deionized water and left to dry at room temperature.

2.3 Study area and sediment sampling

The microbasin of the Marrecas Arroyo ($29^{\circ}03'34''\text{S}$ and $50^{\circ}57'35''\text{W}$) lies within the São Marcos River basin, which is one of the main tributaries of the Taquari-Antas hydrographic basin. Located in a predominantly rural area, this microbasin has an area of 5,512 ha and borders the Faxinal Arroyo basin and the São Francisco de Paula municipality. The arroyo begins close to the locality of Apanhador, in the municipality of Caxias do Sul (Rio Grande do Sul State, Brazil), and is approximately 15 km long [25]. The map in **Fig. 1** shows its location in the regional context at a scale of 1:100,000, and the detailing has a scale of 1:20,000.

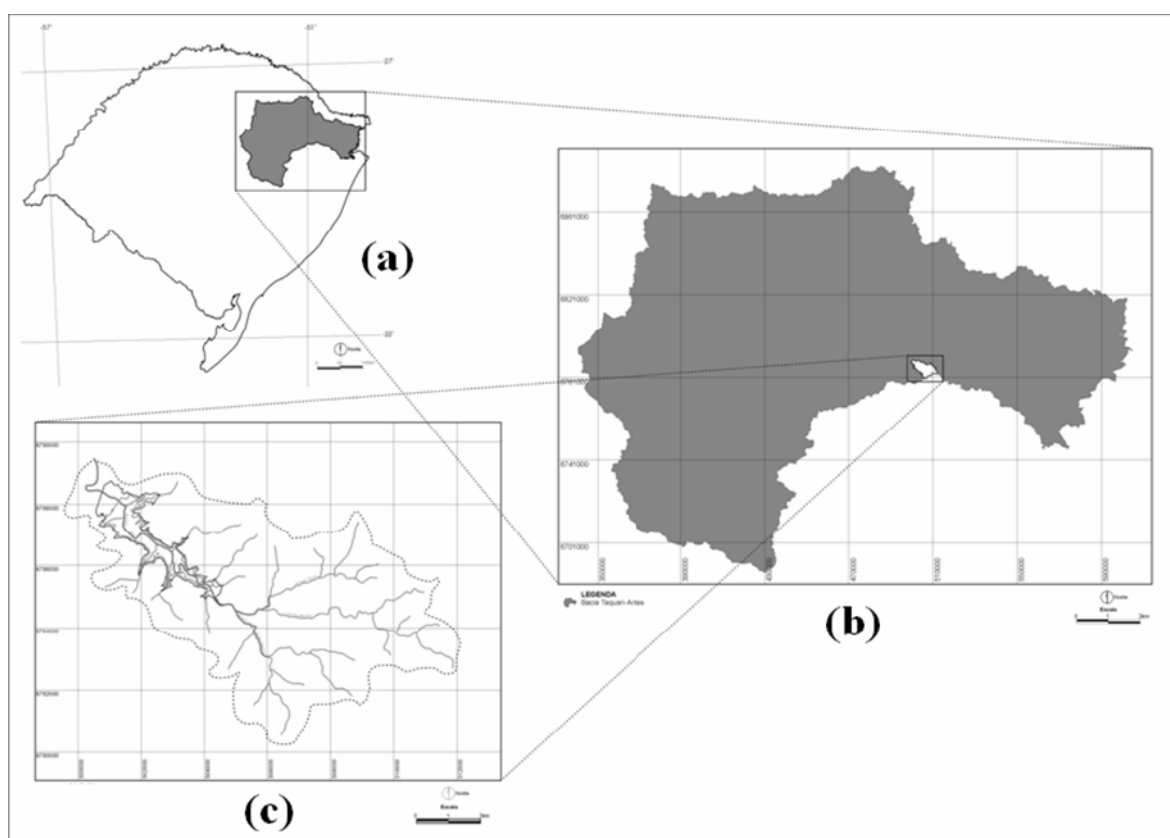


Fig. 1. Localization of the study area: (a) Rio Grande do Sul State (Brazil); (b) Taquari-Antas hydrographic basin; (c) Marrecas Arroyo microbasin.

In this study, four sediment samples (named 1, 2, 3 and 4) were collected directly from the bottom of the stream using a Petersen sampling device. The first and third sampling points are situated in a region of the microbasin where the incidence of vegetation is very low. In these two sites, the vegetation is dominated mainly by grasses and small-sized trees. The second and fourth sampling points, on the other hand, are located in a region of the microbasin surrounded by a dense and well-preserved subtropical rain forest and are consequently strongly influenced by terrestrial OM contributions.

The samples were stored in air-sealed plastic bags at 4°C. Upon reaching the laboratory, all sediments were freeze-dried, ground, sieved, and stored in a desiccator at room temperature, until extraction of the HA was performed.

2.4 Extraction and purification of humic acids

The extraction of HA was performed according to the IHSS protocol and adapted by Giovanela *et al.* [21], mainly in relation to the purification step.

Initially, the pretreated sediment samples were washed with a 0.1 mol/L solution of HCl by mechanical stirring for 1 h. After this procedure, the sample was left to stand for 24 h under refrigeration at 4°C, and the acid supernatant was then separated from the sediment by siphoning. The acid washing aims to promote desorption of humic material which is associated in oxy-hydroxides, silicic acid and clay minerals, and to remove carbonates or exchangeable bases.

The next step consists of washing the sediment sample with a 1.0 mol/L solution of NaOH by mechanical stirring for 1 h. The sample was again left to stand for 24 h under

refrigeration at 4°C, and the alkaline supernatant was then separated by siphoning followed by centrifugation at 3,929 g. The alkaline extract was subsequently acidified with a 6.0 mol/L solution of HCl to pH 2.0 and left to stand for 24 h and at 4°C for complete precipitation of the HA.

Finally, the HA was separated from the supernatant by centrifugation at 3,929 g, purified by dialysis against deionized water until testing negative for chloride (test with AgNO₃ solution of 0.1 mol/L), and then freeze-dried at – 40°C for five days.

2.5 Chemical and spectroscopic characterization of humic acids

The micrographs of the HA were obtained with a Philips XL-30 scanning electron microscope. The freeze-dried samples were previously coated with a thin gold layer in a PS-2 diode sputtering system for 10 min before analysis.

The elemental composition of the HA was determined using a Carlo Erba 1100 CHNS elemental analyzer. Relative quantities of C, H and N were measured directly with the analyzer and the data were recalculated on an ash-free basis. O contribution was estimated as the difference between summed C, H and N concentrations and 100%.

The UV-Vis spectra of the HA solutions (obtained with 5.0 mg of humic material in 250 mL of 0.05 mol/L NaHCO₃) were recorded on a Hewlett-Packard 8453 spectrophotometer in a 1-cm path length quartz cuvette at 770 to 210 nm.

TG curves were recorded using a Shimadzu TGA-50 thermogravimetric analyzer. The HA samples (~10 mg) were placed in platinum crucibles and heated continuously from

25°C to 900°C under nitrogen atmosphere (gas flow 50 cm³/min). A heating rate of 10°C/min was chosen based on previous studies [21, 26–28].

FT-IR spectra were recorded on a Perkin Elmer 16 PC spectrophotometer, with a resolution of 4 cm⁻¹, at 4,000 to 400 cm⁻¹. Pellets were prepared by pressing, under vacuum, a mixture of 1 mg of the HA and 150 mg of KBr (spectroscopy grade).

Solid-state CP-MAS ¹³C NMR spectra were collected on a BRUKER AMX 500 AVANCE spectrometer operating at the ¹³C frequency of 125.8 MHz. The HA samples (~100 mg) were packed into a 4 mm-diameter zircon rotor and spun at the magic angle at a rate of 9 kHz. A conventional cross-polarization pulse sequence was used with a 1 ms contact time. The recycle delay was 4 s and the length of the proton 90° pulse was 4.5 μs. The number of transients collected for each spectrum ranged between 3,000 and 12,000. The sweep width was 50 kHz and the chemical shift scale was referred to tetramethylsilane.

3. Results and discussion

3.1. Morphological analysis

HS have been extensively described by SEM and the observed microstructures are generally dependent on the pH and preparation conditions and include sheets, fibers, short rods, and associations of bundles and networks [23, 24, 29]. In the study reported herein, the HA were observed by SEM in order to evaluate their capacity to form aggregates in the freeze-dried state. The SEM micrographs of the freeze-dried HA are shown in **Fig. 2** and **3**.

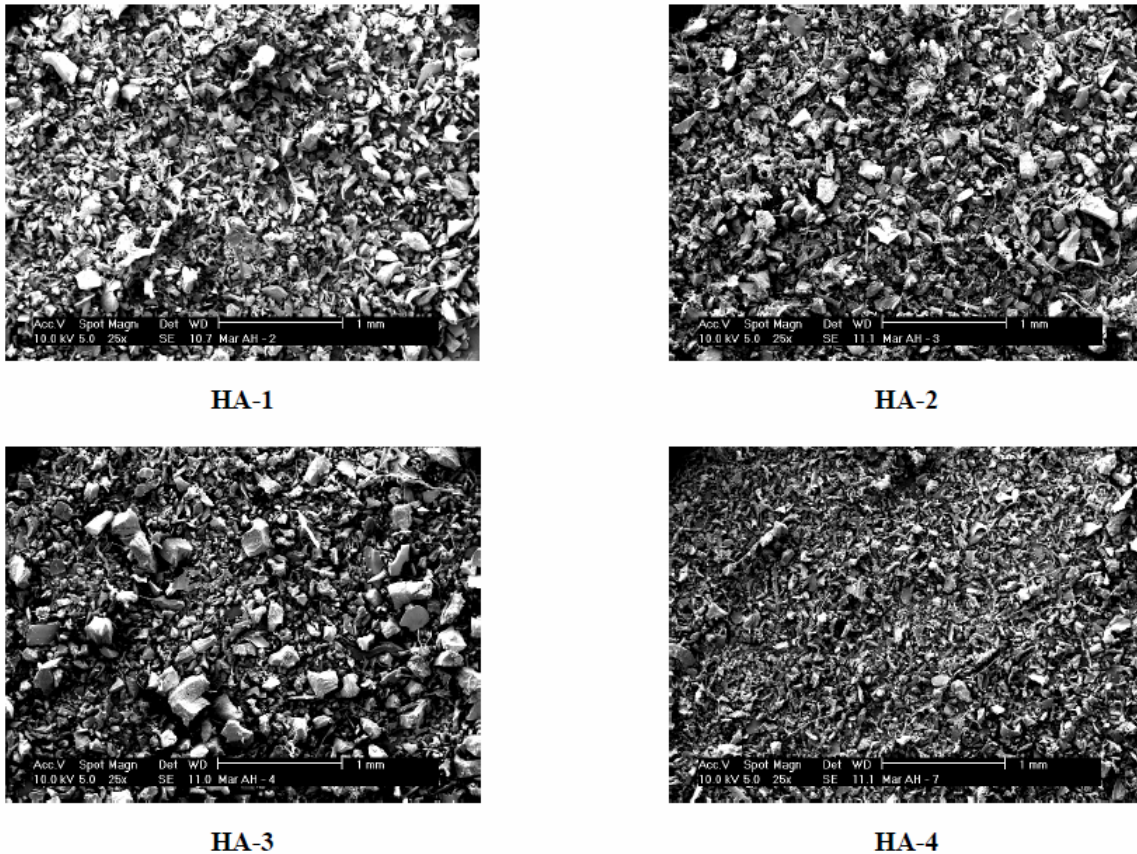


Fig. 2. SEM micrographs of freeze-dried HA (magnification level of 25 ×).

At a low magnification level (25 ×) (**Fig 2**), all samples exhibited similar morphology with no distinct particles but rather a kind of globular-like structure. As can be observed, the particles which comprise the HA-1 and HA-2 samples are relatively more homogeneous than those comprising the HA-3 and HA-4 samples. On the other hand, the HA-3 sample has the greatest heterogeneity in terms of the particle distribution and size, while the HA-4 sample has the smallest particles.

Other slight differences in the aggregation levels could be better detected when the SEM micrographs were observed at relatively high magnification (200 ×) (**Fig. 3**). In this case, it can be verified that the HA aggregates are highly compact, besides having a high level

of microporosity. The sizes and thicknesses of the particles vary from tens to hundreds of micrometers.

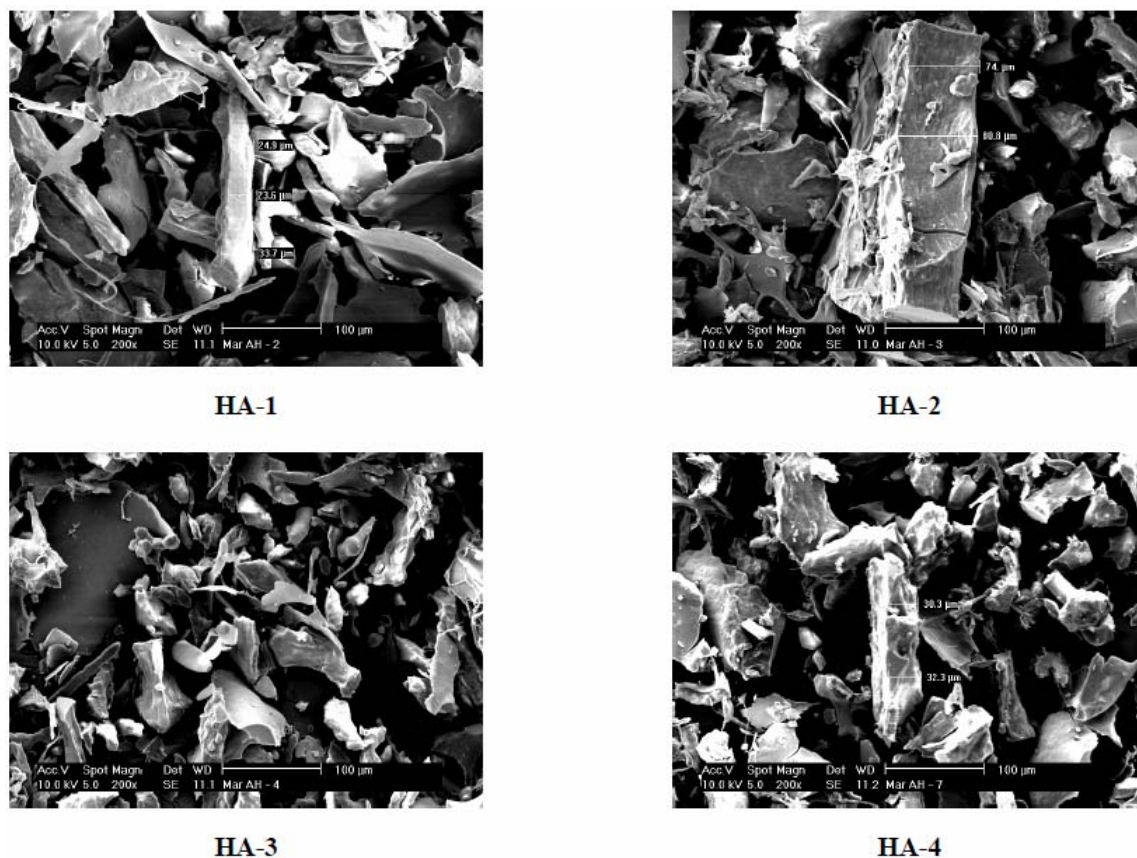


Fig. 3. SEM micrographs of freeze-dried HA (magnification level of 200 ×).

According to Nègre *et al.* [30], aggregation processes leading to the formation of macroaggregates should take place mainly during the freeze-drying step, when the elimination of water increases the interaction between the humic macromolecules. The interaction mechanisms responsible for the formation of aggregates can be weak, aspecific forces, such London and van der Waals forces, whose magnitude is enhanced by the large dimension of the interacting molecules, but more specific and stronger forces such as charge

transfer and hydrogen bonding can also be involved.

It is clearly unrealistic to express any relationship between the chemical structure of HS and their aggregation level, but the formation of large aggregates in HA samples that are rich in O-containing groups suggests that strong interactions, such as charge transfer and hydrogen bonding, promote the cohesion of the particles.

3.2. Elemental analysis

The elemental composition, atomic ratios (H/C and N/C) and ash content of the HA are summarized in **Table 1**.

Table 1 Elemental composition, atomic rations and ash contents of HA

Samples	C (%)	H (%)	N (%)	O (%) ^a	H/C ^b	C/N ^c	Ash content (%)
HA-1	51.27	5.32	2.64	40.77	1.24	22.6	0.7
HA-2	51.06	5.09	2.76	41.09	1.19	21.6	2.6
HA-3	51.14	5.26	2.54	41.06	1.23	23.5	1.1
HA-4	50.38	4.87	2.98	41.77	1.15	19.7	2.0

^a Calculated by subtraction from 100%

^b $H/C = [(\%H / 1.00794) / (\%C / 12.011)]$

^c $C/N = [(\%C / 12.011) / (\%N / 14.0067)]$

The values obtained here are, in general, within the ranges reported in the literature [1, 7, 31]. Due to their complexity, information on the elemental composition of HS is not very

conclusive, and the atomic ratios have preferentially been employed in such studies. The H/C ratio has frequently been associated with the degree of condensation or aromaticity and this, in turn, to the degree of humification, higher H/C values indicating a greater quantity of aliphatic components, typical of less humified materials, in the HS structures [1].

The H/C values in all HA samples are greater than one, indicating that these samples probably originate from vascular plant material rather than algal or bacterial OM [6, 8]. Moreover, the values observed (**Table 1**) suggest a greater proportion of condensed structures in the HA-2 and HA-4 samples, and consequently a greater quantity of aromatic structures, in relation to the HA-1 and HA-3 samples. The sampling points 2 and 4 are, in fact, situated in a region of the microbasin where medium and large-sized trees predominate. On decomposing, part of this vegetation, which is rich in lignins, is incorporated into the sediments and, as a result of this process, the HA of these locations have a slightly more accentuated aromatic character than those of the other two locations, where the incidence of vegetation was very low.

The C/N ratio has also been considered as an indicator of the sources of HS in natural systems. Nonvascular aquatic plants have a low C/N ratio, typically between 2.0 and 10, whereas vascular land plants, which contain cellulose, lignin and tannins, have ratios of 20 and higher [32, 33]. The C/N ratios in this study ranged from 19.7 to 23.5 (**Table 1**). These values are relatively high, once again indicating that terrestrial vascular plants are the dominant contributors to our samples. As previously mentioned, all sites where the sediments were collected receive more or less OM from terrestrial sources and, for this reason, these trends were to be expected.

3.3. UV-Visible spectroscopy

The UV-Vis spectra of the HA are shown in **Fig. 4**. As expected, and in agreement with previously published data [34–36], they are rather featureless and increase in intensity almost consistently from 770 to 210 nm.

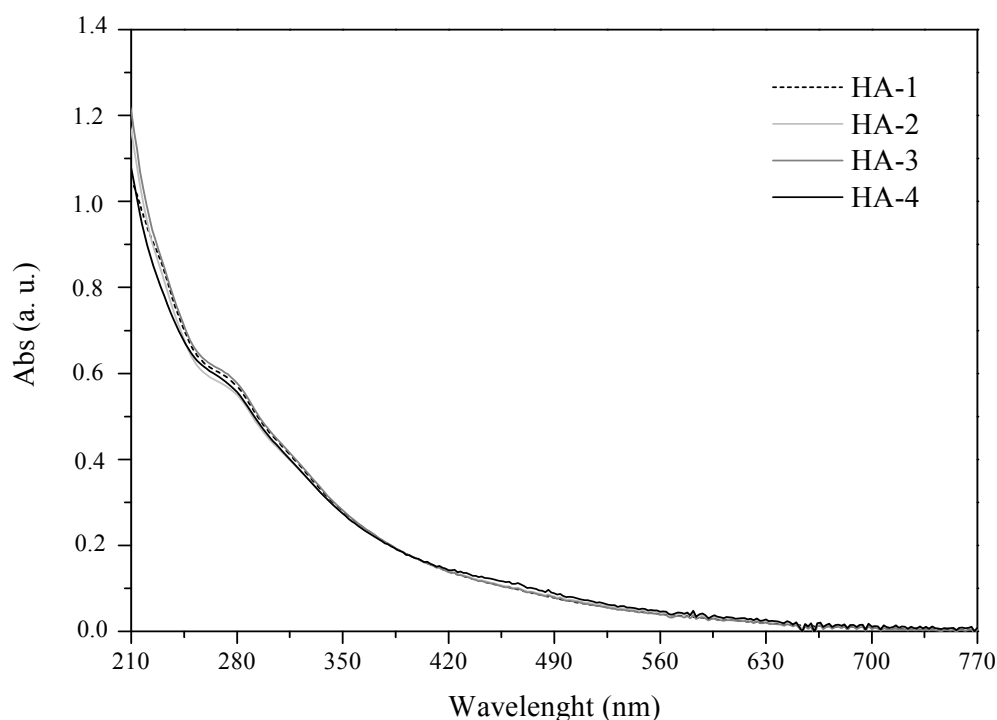


Fig. 4. UV-Vis spectra of HA.

A discreet “shoulder” can be also observed at around 280-270 nm in all spectra. According to several authors [37, 38], this electronic transition is due to overlapping absorbance of a large number of chromophores present in the humic core. In general, the chromophores responsible for the absorption in the UV region are principally phenolic arenes, benzoic acids, aniline derivatives, polyenes, and polycyclic aromatic hydrocarbons with two or more rings.

The absorbance in the visible region, on the other hand, is more complicated to explain, although some authors have suggested that it could principally be related to extended conjugation in aliphatic or polyaromatic structures, quinoid structures and keto-enol-systems, as well as to the presence of metal complexes and/or inter-, or intramolecular donor–acceptor complexes [35, 39–41].

Table 2 shows the data related to the E_4/E_6 ratio and the $\Delta\log K$ coefficient for HA samples. As can be observed, the values for E_4/E_6 ratio range from 5.64 to 7.80. This parameter has been widely used in HS studies as an indicator of humification, this ratio decreasing with increases in the degree of condensation [34, 37, 40–47]. The values in **Table 2** again suggest that HA-2 and HA-4 appear to be slightly richer in aromatic structures than the HA-1 and HA-3 samples.

Table 2 UV-Visible spectral properties of HA

Samples	E_4/E_6 ^a	$\Delta\log K$ ^b
HA-1	7.80	0.77
HA-2	5.87	0.72
HA-3	7.71	0.79
HA-4	5.64	0.70

^a $E_4/E_6 = \text{Abs}_{465 \text{ nm}} / \text{Abs}_{665 \text{ nm}}$

^b $\Delta\log K = \log \text{Abs}_{400 \text{ nm}} - \log \text{Abs}_{600 \text{ nm}}$

With regard to the $\Delta\log K$ coefficient, the values were located at around 0.75.

According to Kumada [39], the degree of condensation of HA increases with decreasing $\Delta\log K$

values. Similar behavior to that observed for the E_4/E_6 is again reproduced for the same samples (HA-2 and HA-4), when this parameter is evaluated. Besides this information, this coefficient can also be used to classify the HA. In general, they can be grouped in four different classes: A, B, Rp and P. In our case (**Table 2**), all samples are of type B. These particular HA samples have a weak “shoulder” of absorption at 280-270 nm and $\Delta\log K$ values of 0.60 to 0.80. Type A HA samples do not present characteristic absorption bands and the $\Delta\log K$ values are lower than 0.60. HA of the Rp type present the same spectrum as that of type B, but with higher $\Delta\log K$ values (between 0.80 and 1.10). Finally, the HA with characteristic absorptions in the visible region at 615, 570, and 450 nm are considered as type P. These findings appear to be consistent with the elemental analysis data (**Table 1**).

3.4. Thermal analysis

Fig. 5 shows the TG and DTG profiles for the HA samples studied. As can be observed, the profiles are similar for all samples. In general, the thermal decomposition proceeds through three main stages. The first stage occurs in the temperature range between 60°C and 90°C and correspond to the evaporation of water incorporated in or adsorbed onto the HA, being accompanied by a slight weight loss (around 6.7%). The second and third stages are more evident and can be observed in the temperature range of 260°C to 350°C, being accompanied by weight losses of approximately 16% and 30%, respectively. After that, weight loss remains steadily, without further observable features, until the highest temperature measured (900°C).

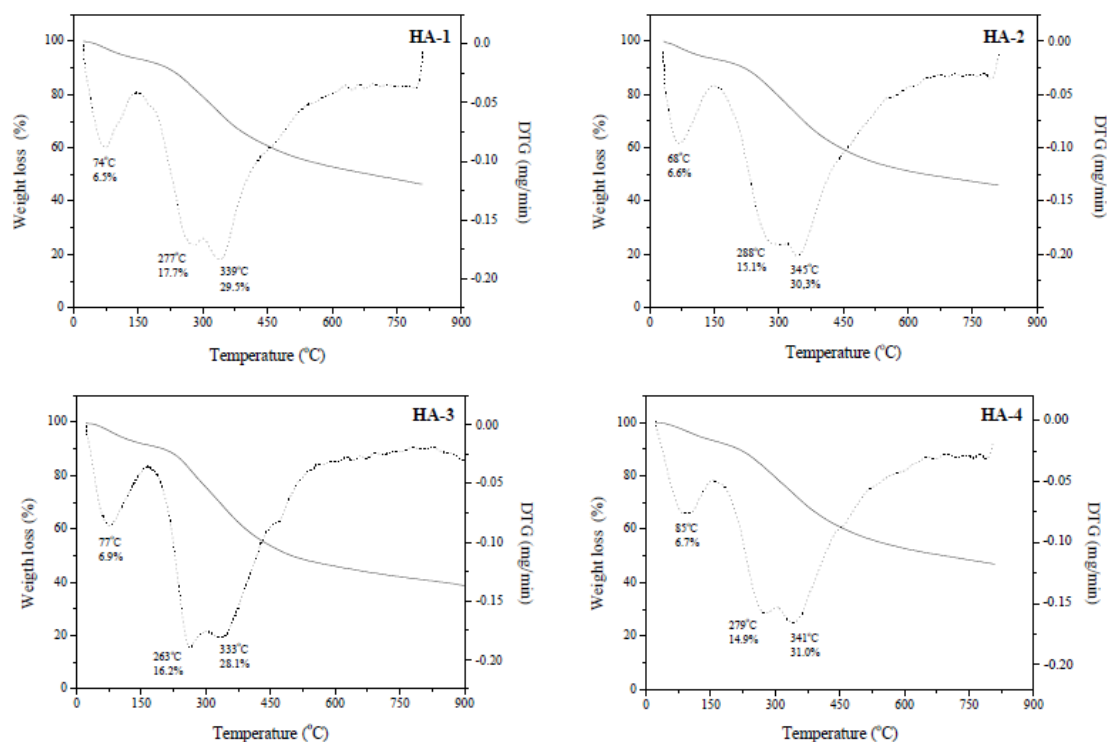


Fig. 5. TG (—) and DTG (----) curves of HA.

It has commonly been reported that the decline between 200°C to 400°C observed in TG curves for humic materials is due to the loss of polar functional groups and the combustion of aliphatic structures derived from the decomposition of plants and animals, as well as from different pedogenic sources [48, 49].

Schnitzer and Hoffman [95], for example, showed that phenolic OH and COOH groups were eliminated at between 250°C and 400°C. Campanella and Tomassetti [26] monitored the thermal degradation of HS with FT-IR spectroscopy and reported that, for soil extracts, decarboxylation and unsaturation losses occur at around 280°C. Ioselis *et al.* [42] also observed the decomposition of carboxylic, phenolic, carbonyl and alcoholic groups in HS at around 300°C.

A fourth event at around 500°C can also be observed in the DTG curves of these humic materials. This has commonly been associated with the depletion of aromatic structures [50]. This type of event, however, has been observed with greater frequency in HS derived from highly humified materials, such as coals and lignites, which have a large quantity of aromatic structures that are consequently more resistant to thermal decomposition [51, 52].

In our samples, only the first three events were observed, suggesting that these HA do not have many aromatic structures in their composition, at levels which can be detected by this technique. Also, samples HA-2 and HA-4 seem to be slightly more resistant to thermal degradation than HA-1 and HA-3, since the decomposition of the former samples occurs at relatively higher temperatures.

This information appears to be consistent with the thermogravimetric index (TGI) (**Table 3**). This parameter can be obtained from the quotient between the mass losses observed in the third and second events, respectively. According to many authors [53, 54], the TGI has been frequently used in TG in order to evaluate the thermal stability of HS. The data confirmed that HA-2 and HA-4 are thermally more stable (higher TGI values) than the HA-1 and HA-3 samples (lower TGI values).

Table 3 Thermogravimetric index (TGI) of HA

Samples	TGI ^a
HA-1	1.67
HA-2	2.01
HA-3	1.73
HA-4	2.08

^a TGI = weight loss (%) at 305-650°C / weight loss (%) at 105-305°C

3.5. FT-IR spectroscopy

The FT-IR spectra of the HA are shown in **Fig. 6**. As can be observed, they present typical HS features [10, 11, 55, 56] and are very similar. The band at around 3400-3000 cm^{-1} is the broadest for all samples. This band, in HS, has been attributed to O-H stretching of alcohols and/or phenols and N-H stretching of amines and/or amides [57].

A high degree of saturation in these HA samples can be inferred by observing the 2940-2850 cm^{-1} absorption range. For all samples, two bands appear in this region (at around 2926 and 2855 cm^{-1}). These bands are attributed to the asymmetric and symmetric C-H stretching of methyl and methylene groups of aliphatic and nonstrained cyclic hydrocarbons [8]. This feature is in agreement with the ^{13}C NMR data which revealed a high percentage of aliphatic carbons in all samples studied.

Within the 1720 to 1600 cm^{-1} wavenumber range, a systematic difference in the behavior can be observed in our spectra. The C=O stretching of COOH and other carbonyl groups (absorption band around 1709 cm^{-1}) is, in general, less pronounced than the second band located around 1639 cm^{-1} . The latter absorption band has several assignments including aromatic C=C stretching, amide group C=O stretching and N-H bending. For single compounds, carbon-carbon stretching usually appears at about 1650 cm^{-1} , but it is shifted to around 1600 cm^{-1} by conjugation. Substituted or unsubstituted amides show the C=O band (amide I) in the 1660-1640 cm^{-1} region and the N-H bending (amide II) at 1540-1500 cm^{-1} [58, 59].

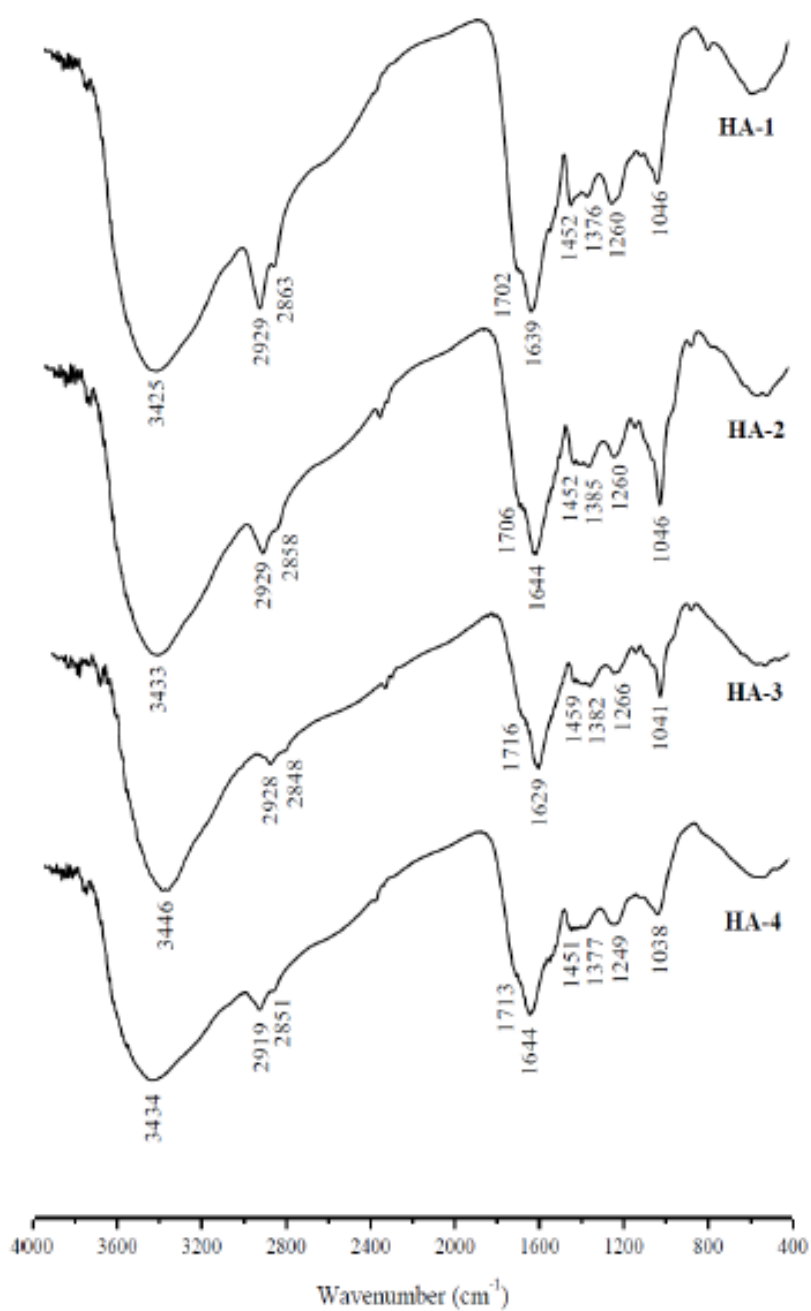


Fig. 6. FT-IR spectra of HA.

In HS, all these types of vibrations are expected to exist, and their corresponding frequency signals might be overlapped in this region, the shifts to the right or left being a result of the relative influence of each group. The aromatic C=C absorption, for example, is

thought to be responsible for this band in lignin derivative materials whereas the amide I band might be prevalent for proteinaceous materials [11]. In our case, the band observed at around 1640 cm^{-1} seems to be associated mainly with the vibrations of C=C groups. Furthermore, none of the spectra showed the band characteristic of amide II. This band has generally been associated with polypeptide-derived structures, which are apparently present in low quantities in the HA samples studied. This information is reinforced by the C/N ratio values (**Table 1**) which are high for all samples.

In the region of $1460\text{-}1370\text{ cm}^{-1}$, the absorption bands corresponding to C-H bending of CH_3 and C-H deformation of CH_2 and CH_3 groups were observed. Additional bands also appeared at $1260\text{-}1250\text{ cm}^{-1}$ in all FT-IR spectra, which correspond to the C-O stretching of aryl ethers and phenols [60].

Finally, the band at around $1050\text{-}1040\text{ cm}^{-1}$ has been assigned to C-O stretching of polysaccharides or polysaccharide-like components [61–63]. The higher relative intensities of these bands in the FT-IR spectra of HA may be related to the decomposition of cellulose, which is also found in higher plants.

3.6. Solid-state CP-MAS ^{13}C NMR

The CP-MAS ^{13}C NMR spectra of HA and the relative abundances of the different classes of carbon atoms are presented in **Fig. 7** and **Table 4**, respectively. Regarding the FT-IR data, the samples yielded similar spectra. Five chemical shift regions were assigned to these spectra: $R_1 = 0\text{-}45\text{ ppm}$ (aliphatic C), $R_2 = 45\text{-}110\text{ ppm}$ (O-substituted alkyl C), $R_3 = 110\text{-}160\text{ ppm}$ (aromatic C), $R_4 = 160\text{-}190\text{ ppm}$ (carboxylic acid C), and $R_5 = 190\text{-}220\text{ ppm}$

(carbonyl C) [64]. These major spectral bands are consistent with those observed for soil and aquatic HS, although the relative intensities of the peaks can vary greatly among samples [10, 65, 66].

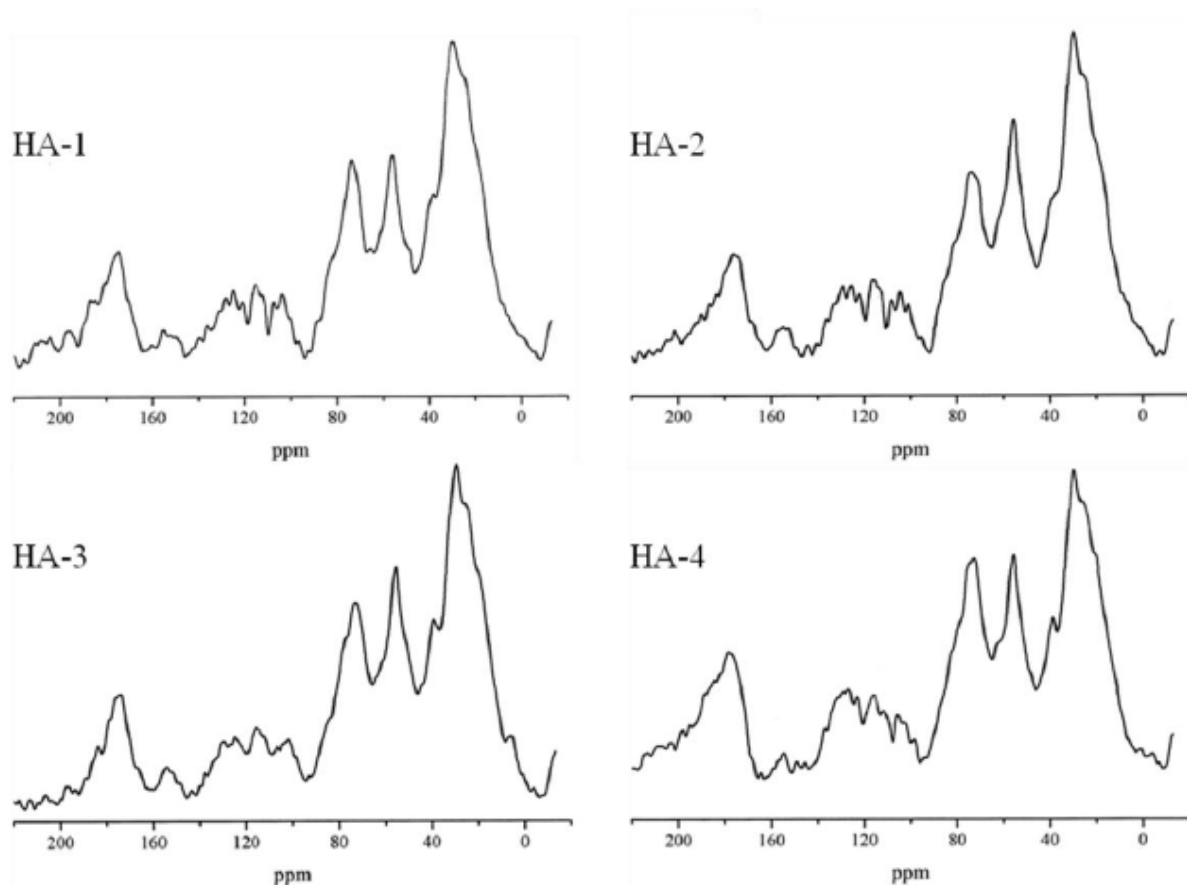


Fig. 7. Solid state CP-MAS ^{13}C NMR spectra of HA.

The aliphatic C region is dominated by the peaks at 24, 29 and 33 ppm that arise from the alkyl carbon components, such as methyl, methylene and methine carbons [8]. The peak centered at 29 ppm is well defined and prominent in all HA spectra, suggesting a relatively high amount of aliphatic components in their structures. This result is confirmed by the percentage of aliphatic C, which varies from 35.3 to 37.4% (**Table 4**). The data are

consistent with results for the elemental and infrared analysis and suggest that the HA are rich in alkyl-like matter. As mentioned earlier, the H/C ratios are greater than one (**Table 1**) and the band associated with the C-H stretching of methyl and methylene groups is well defined in all FT-IR spectra (**Fig. 6**).

In the O-substituted alkyl C region two well-resolved peaks at 55 and 71 ppm and a small peak at 102 ppm are evident in the spectra of all HA samples. The peak at 55 ppm has been assigned to methoxy groups associated with lignin and lignin-like products [67]. The peak at 71 ppm is thought to correspond to the carbon rings of polysaccharides, and the signal at 102 ppm has been attributed to anomeric carbons in polysaccharides. This latter resonance may also indicate nonprotonated aromatic carbons in tannins [68]. The percentage of O-substituted alkyl C in this region varies from 40.1 to 41.7% (**Table 4**). The percentages obtained for this region are also high, confirming that the HA samples are rich in portions derived from higher plants.

Table 4 Integrated areas of the main spectral bands of solid-state CP-MAS ^{13}C NMR spectra of HA.

Samples	R ₁ (%) ^a	R ₂ (%) ^b	R ₃ (%) ^c	R ₄ (%) ^d	R ₅ (%) ^e
HA-1	37.4	41.4	11.6	8.5	1.1
HA-2	36.9	40.1	12.0	9.1	1.9
HA-3	37.0	41.7	11.3	8.8	1.2
HA-4	35.3	40.5	12.9	10.6	0.7

^aR₁ = (A₁/A_T) . 100 %, where A₁ is the value of the area obtained in the range of 0-45 ppm and A_T is the value of the area obtained in the range of 0-220 ppm;

^bR₂ = (A₂/A_T) . 100 %, where A₂ is the value of the area obtained in the range of 45-110 ppm and A_T is the value of the area obtained in the range of 0-220 ppm;

^c $R_3 = (A_3/A_T) \cdot 100 \%$, where A_3 is the value of the area obtained in the range of 110-160 ppm and A_T is the value of the area obtained in the range of 0-220 ppm;

^d $R_4 = (A_4/A_T) \cdot 100 \%$, where A_4 is the value of the area obtained in the range of 160-190 ppm and A_T is the value of the area obtained in the range of 0-220 ppm;

^e $R_5 = (A_5/A_T) \cdot 100 \%$, where A_5 is the value of the area obtained in the range of 190-220 ppm and A_T is the value of the area obtained in the range of 0-220 ppm.

In the 110-160 ppm region, the peak at 129 ppm has been attributed to unsaturated carbons or aryl-C with protonated aromatic C [66]. Also, in this region, a minor peak at 151 ppm, which is indicative of carbon bonded to phenolic OH [69], is present for most of our samples. The percentage of aromatic carbon varies from 11.3 to 12.9% (**Table 4**). This result is again in agreement with the elemental and FT-IR data, which show strong signals of aliphatic moieties in their structures.

In the 160 to 190 ppm region, all HA samples exhibit a peak at around 170 ppm, which is characteristic of carboxyl, amide and ester functionalities [8]. The percentage of C in this region is low and varies from 8.5 to 10.6%. The ketonic C=O peaks (~ 200 ppm) are very weak in all spectra and vary from 0.7 to 1.9% in this set of samples.

Finally, comparing the ^{13}C -NMR spectra for the samples clearly reveals that terrestrial OM plays an important role in the composition of the HA samples studied. The general trend observed is that the higher the terrestrial influence the higher the aromatic carbon percentage of the samples. This information complements the results obtained from applying the other analysis techniques.

4. Conclusions

The results for the characterization of the HA samples using SEM, elemental analysis, TG, and UV-Vis, FT-IR, and CP/MAS ^{13}C -NMR spectroscopies are basically in agreement with each other.

Although all samples originated from the same environment, the data showed that the HA have distinct chemical and spectroscopic properties, and that the location and characteristics of the sampling points from which the sediments were collected contributed directly to the differences observed. Furthermore, vascular plant matter is probably the main contributor to the composition of these samples.

Acknowledgments

This work was supported by the Conselho Nacional de Pesquisa e Desenvolvimento (CNPq, Brazil, Project No. 481824/2007-3) and Coordenação de Aperfeiçoamento de Pessoal de Nível Superior (CAPES, Process BEX 4144/09-0). The careful reviews were considerably helpful in improving this manuscript.

References

- [1] F. J. Stevenson, *Humus Chemistry: Genesis, Composition, Reactions*, Wiley & Sons, New York, 1994.
- [2] J. I. Hedges, *Mar. Chem.* 39 (1992) 67.
- [3] R. Sutton, G. Sposito, *Environ. Sci. Technol.* 39 (2005) 9009.
- [4] A. Cozzolino, P. Conte, A. Piccolo, *Soil Biol. Biochem.* 33 (2001) 563.
- [5] R. A. Bourbonniere, P. A. Meyers, *Can. J. Spectrosc.* 23 (1978) 35.
- [6] J. A. Rice, P. MaCarthy, *Org. Geochem.* 17 (1991) 635.
- [7] N. Belzile, H. A. Joly, H. Li, *Can. J. Chem.* 75 (1997) 14.
- [8] M. M. D. Sierra, M. Giovanela, E. Parlanti, V. I. Esteves, A. C. Duarte, A. Fransozo, E. J. Soriano-Sierra, *J. Coast. Res.* 42 (2005) 370.
- [9] H. Mengchang, S. Yehong, L. Chunye, *J. Environ. Sci.* 20 (2008) 1294.
- [10] A. Fernandes, M. Giovanela, V. I. Esteves, M. M. D. Sierra, *J. Mol. Struct.* 971 (2010) 33.
- [11] M. Mecozzi, M. Amici, E. Pietrantonio, G. Romanelli, *Ultrasonics Sonochem.* 9 (2002) 11.
- [12] Y. Chen, N. Senesi, M. Schnitzer, *Soil Sci. Soc. Am. J.* 41 (1977) 352.
- [13] P. Lassen, L. Carlsen, P. Warwick, A. Randall, R. Zhao, *Environ. Int.* 20 (1994) 127.
- [14] P. Conte, A. Piccolo, B. van Lagen, P. Buurman, P.A. de Jager, *Geoderma* 80 (1997) 339.
- [15] P. Conte, A. Piccolo, *Environ. Sci. Technol.* 33 (1999) 1682.
- [16] J. Peuravuori, *Int. J. Environ. Anal. Chem.* 76 (2000) 179.

- [17] M. A. Wilson, R. J. Pugmire, D. M. Grant, *Org. Geochem.* 5 (1983) 121.
- [18] C. M. Preston, B. A. Blackwell, *Soil Sci.* 139 (1985) 88.
- [19] A. M. Vassalo, M. A. Wilson, P. J. Collin, J. M. Oades, A. G. Waters, R. L. Malcolm, *Anal. Chem.* 59 (1987) 558.
- [20] E. W. D. Huffman, H. A. Stuber, *Analytical methodology for elemental analysis of humic substances. Humic Substances in Soil, Sediment and Water: Geochemistry, Isolation and Characterization* (G. R. Aiken, D. M. McKnight, R. L. Wershaw, P. MacCarthy, eds.), Wiley, New York, 1985.
- [21] M. Giovanela, E. Parlanti, E. J. Soriano-Sierra, M. S. Soldi, M. M. D. Sierra, *Geochem. J.* 38 (2004) 25.
- [22] Y. Chen, M. Schnitzer, *Soil Sci. Soc. Am. Proc.* 40 (1976) 682.
- [23] M. A. Vicente, M. Robert, C. R. Acad. Sci. Paris 292 (1981) 1161.
- [24] K. H. Tan, *Soil Sci. Soc. Am. J.* 49 (1985) 1185.
- [25] M. Antunes, D. B. Dillon, J. S. Crespo, M. Giovanela, *Geochem. Brasiliensis* 22 (2008) 178.
- [26] L. Campanella, M. Tomassetti, *Thermochim. Acta* 170 (1990) 67.
- [27] A. Piccolo, F. J. Stevenson, *Infrared evidence of thermal decarboxylation in potassium salts of humic substances. Humic Substances in the Global Environment and Implications on Human Health* (N. Senesi, T. M. Miano, eds.), Elsevier, Amsterdam, 1994.
- [28] V. I. Esteves, A. C. Duarte, *Mar. Chem.* 63 (1999) 225.
- [29] Y. Chen, M. Schnitzer, *Soil Sci. Soc. Am.* 40 (1976) 682.

- [30] M. Nègre, P. Leone, J. Trichet, C. Défarge, V. Boero, M. Gennari, *Geoderma* 121 (2002) 1.
- [31] M. A. Rashid, *Geochemistry of Marine Humic Compounds*. Springer-Verlag, New York, 1985.
- [32] P. A. Meyers, R. Ishiwatari, *Org. Geochem.* 20 (1993) 867.
- [33] X. Q. Xu, J. V. Hanna, W. D. Johnson, *Applied Geochem.* 15 (2000) 1019.
- [34] Y. P. Chin, G. Aiken, E. Loughlin, *Environ. Sci. Technol.* 28 (1994) 1853.
- [35] A. U. Baes, P. R. Bloom, *Soil Sci. Soc. Am. J.* 54 (1990) 1248.
- [36] G. V. Korshin, C. W. Li, M. M. Benjamin, *Water Res.* 31 (1997) 1787.
- [37] J. Peuravuori, K. Pihlaja, *Anal. Chim. Acta* 337 (1997) 133.
- [38] U. Fooker, G. Liebezeit, *Mar. Geol.* 164 (2000) 173.
- [39] K. Kumada, *Chemistry of Soil Organic Matter*, Japan Scientific Societies Press, Tokyo, 1987.
- [40] F. J. Stevenson, *Humus Chemistry: Genesis Composition Reaction*, Wiley-Interscience, New York, 1982.
- [41] L. P. Canellas, G. A. Santos, *Humosfera: Tratado Preliminar sobre a Química das Substâncias Húmicas*, Campos dos Goytacazes, Biblioteca do CCTA / UENF, 2005.
- [42] P. Ioselis, Y. Rubinsztain, R. Ikan, Z. Aizenshtat, M. Frenkel, *Org. Geochem.* 8 (1985) 95.
- [43] Y. Inbar, Y. Chen, Y. Hadar, *Soil Sci. Soc. Am. J.* 54 (1990) 1316.
- [44] J. Chen, B. Gu, E. J. Leboeuf, H. Pan, S. Dai, *Chemosphere* 48 (2002) 59.

- [45] J. Pajczkowska, A. Sułkowska, W. W. Sułkowski, M. Jedrzejczyk, *J. Mol. Struct.* 651-653 (2003) 141.
- [46] J. Cieslewicz, S. S. Gonet, *Aquat. Sci.* 66 (2004) 178.
- [47] S. S. Fong, M. Mohamed, *Org. Geochem.* 38 (2007) 967.
- [48] H. R. Schulten, P. Leinweber, *Eur. J. Soil Sci.* 50 (1999) 237.
- [49] J. D. Sheppard, D. W. Forgeron, *Fuel* 66 (1987) 232.
- [50] D. Montecchio, O. Francioso, P. Carletti, D. Pizzeghello, S. Chersich, F. Previtali, S. Nardi, *J. Thermal Anal. Cal.* 83 (2006) 393.
- [51] P. Leinweber, R. Schulten, C. Horte, *Thermochim. Acta* 200 (1992) 151.
- [52] A. N. Fernandes, Tese de Doutorado, Universidade Federal de Santa Catarina, Florianópolis, 2007, p. 149.
- [53] Benites, V. M., Mendonça, E. S., Schaefer, C. E. G. R., Novotny, E. H., Reis, E. L., Ker, J. C., *Geoderma* 127 (2005) 104.
- [54] Cunha, T. J. F., Madari, B. E., Benites, V. M., Canellas, L. P., Novotny, E. H., Moutta, R. O., Trompowski, P. M., Santos, G. A., *Acta Amazonica* 37 (2007) 91.
- [55] L. T. Shirshova, E. A. Ghabbour, G. Davies, *Geoderma* 133 (2006) 204.
- [55] V. I. Esteves, M. Otero, A. C. Duarte, *Org. Geochem.* 40 (2009) 942.
- [56] M. C. Scapini, V. H. Conzonno, V. T. Balzaretto, A. F. Cirelli, *Aquatic. Sci.* 72 (2010) 1.
- [57] L. J. Bellamy, *The Infrared Spectra of Complex Molecules*, 3rd ed., Chapman and Hall, London, 1975.
- [58] R. M. Silverstein, F. X. Webster, D. J. Kiemle, *Identificação Espectrométrica de Compostos Orgânicos*, LTC, Rio de Janeiro, 2006.

- [59] R. T. Morrison, R. N. Boyd, Química Orgânica, Fundação Calouste Gulbequian, Lisboa, 1991.
- [60] A. Mendonça, A. C Duarte, E. B. H. Santos, Biogeochem. 69 (1994) 159.
- [61] F. J. Stevenson, K. M. Goh, Geochim. Cosmochim. Acta 35 (1971) 471.
- [62] G. Peshel, T. Wildt, Water Res. 22 (1988) 105.
- [63] K. Kalbitz, W. Geyer, S. Geyer, Biogeochem. 47 (1999) 219.
- [64] R. L. Malcolm, Spectroscopic Approaches. In: M.H.B. Hayes, P. MacCarthy, R. L. Malcolm, R.S. Swift (Eds.), Humic Substances II. In Search of Structure. John Wiley & Sons, Chichester, 1989.
- [65] R. L. Cook, C. H. Langford, Environ. Sci. Technol. 32 (1998) 719.
- [66] J. D. Mao, W. G. Hu, K. Schmidt-Rohr, G. Davies, E. A. Ghabbour, B. Xing, Soil Sci. Soc. Am. J. 64 (2000) 873.
- [67] P. G. Hatcher, R. Rowan, M. A. Mittingly, Org. Geochem. 2 (1980) 77.
- [68] P. F. Van Bergen, P. G. Hatcher, J. J. Boon, M. F. Collinson, J. W. De Leeuw, Phytochem. 45 (1997) 601.
- [69] B. C. Liang, E. G. Gregorich, M. Schnitzer, H. R. Schulten, Soil Sci. Soc. Am. J. 60 (1996) 1758.